JOURNAL OF MATERIALS SCIENCE 11 (1976) 1697–1710

The influence of transverse shear on the static flexure and Charpy impact response of hybrid composite materials

DONALD F. ADAMS*, A. KEITH MILLER
Department of Mechanical Engineering, University of Wyoming, Laramie, Wyoming, USA

Classical laminated anisotropic plate theory, extended to include the effects of transverse shear, is applied to the three-point beam bending problem, to determine the deflections under load, hence flexural modulus, and also the energy absorbed by the beam to the point of peak load, i.e. to first failure. A standard unnotched Charpy impact specimen configuration, constructed of a multi-lamina hybrid composite material, is analysed. Transverse shear is shown to have a significant influence on the response. The analytical results are compared with experimental data, for both impact and static loadings. A definite loading rate dependence is observed.

1. Introduction

A previous investigation [1, 2] had shown that inclusion of third-phase supplementary reinforcing fibres within graphite/epoxy composite materials can significantly increase the impact properties of these materials. A considerable amount of experimental data was gathered, some of which indicated that as much as a 550% increase in impact resistance can be gained by incorporating S glass fibres into the basic graphite/epoxy material [1, 2].

In a continuing effort to further improve the impact properties of graphite/epoxy composites, several different third-phase supplementary materials were used in a more recent study [3, 4]. This investigation also included an analytical study of the impact behaviour of these materials [5]. In these studies, composites containing third-phase reinforcing materials have been termed hybrid composites, a term which will also be used in this paper.

The effects of specimen geometry and rate of loading on the Charpy impact response of hybrid composites were also studied in the most recent investigation [3, 4]. Some very interesting results have been obtained, which indicate that both the rate of loading and the specimen geometry of the impact specimen have profound effects on the test results. An analysis of this response, which is presented here, indicates that the shear stress developed within the test specimen is a major parameter, causing the geometry of the specimen to be a critical factor in the test results.

2. Material description

The basic graphite/epoxy composite system was fabricated from Modulite 5206 graphite/epoxy prepreg. Modulite 5206 consists of unidirectional, collimated Modmor II graphite fibres impregnated with Narmco 1004 epoxy resin. The prepreg was purchased from Whittaker Corporation in Type 2 (broadgoods) form. This material is fully characterized, and well-documented mechanical strength data exist for this material [1, 2], providing a reference point for the evaluation of data generated within the present study.

Four supplementary, third-phase reinforcing materials were used in the present study. These supplementary materials included Style 120 glass cloth, 200 mesh aluminium wire, 0.13 mm titanium foil, and S2 glass yarn. The aluminium mesh, 120 glass cloth and S2 glass yarn were impregnated with the same Narmco 1004 resin system used in the baseline Modulite 5206 material.

* Also Consultant, Aeronutronic Division, Aeronutronic Ford Corporation, Newport Beach, California, USA.

The third-phase materials were added to the basic laminated system as discrete plies dispersed through the laminate thickness.

The construction of the Modulite 5206 control laminate consisted of a basic thirteen-ply repeating set. The orientation of the fibres was arranged with two plies at 0°, plies at +45° and −45°, two plies at 0°, one ply at 90°, two plies at 0°, plies at −45° and +45°, and two plies at 0°. In accordance with [6], the above composite laminate is identified as $[0_2/\pm45/0_2/90/0_2/\mp45/0_2]$. Specimens of two different thicknesses were fabricated. Thick specimens consisted of four sets of the basic orientation, and thin specimens consisted of only one set of the basic lay-up pattern.

The hybrid composite systems were fabricated using a basic fifteen-ply repeating set. The plies were consonantly aligned in the following array: $[0/0^t/\pm45/0^t/0_2/90/0_2/0^t/\mp45/0^t/0]$. The plies without superscripts consisted of Modulite 5206 graphite/epoxy, while superscript t indicates plies of one of the third-phase reinforcing materials. The hybrid test specimens were also fabricated as thick and thin specimens, the thick specimens consisting of four of the basic fifteen-ply sets, while the thin specimens were composed of only one set. A more detailed description of the fabrication procedure and the mechanical properties of the various constituent materials can be found in [3].

3. Test procedures

Instrumented Charpy impact tests, which yield a continuous load–time history of a standard Charpy impact test, were performed on all of the material systems discussed above. This load–time trace allows the Charpy impact test to become a dynamic three-point flexure test, i.e. it makes available a complete loading history of the particular specimen just as a static flexure test does. Therefore, in order to recognize the parameters which differentiate the behaviour of hybrid composites when subjected to quasi-static versus dynamic flexural loadings, "static" three-point flexure tests were also performed on test specimens of dimensions identical to the Charpy specimens. All impact and flexural test specimens were unnotched.

The support span used in the flexure test was the same as that for a standard Charpy impact test, i.e. 40 mm (1.57 in.). The specimens referred to here as thick specimens were of approximately the same dimensions as a standard Charpy impact specimen, i.e. 55 mm long and 10 mm square in cross-section. Results of a previous investigation [1, 2, 5] indicated that the geometry of a standard Charpy impact specimen has an influence on the test results. Therefore, thin specimens were also fabricated and tested in both impact and static flexure. Because of their smaller thickness, the thin specimens had a much larger (approximately four times greater) support span-to-specimen thickness ratio than did the specimens which were of approximately the dimensions of a standard Charpy specimen (the thick specimens). It has become evident from the present static flexural test data that the geometry of the test specimen does indeed have a profound effect on the test results. Further detailed discussion of phenomena possibly responsible for the type of behaviour observed, based on the analysis to be presented here, is contained in the following sections.

4. Analysis of flexure stresses

The typical load–time trace obtained from an instrumented Charpy impact test may be partitioned into two regions: the initial region of increasing load (to the point of peak load), and the region following peak load. It has commonly been assumed, at least until the present time, that the point of peak load is contiguous with the event of first fracture.

The load–time trace of an instrumented Charpy impact test may easily be converted to a load–defection trace by simply multiplying the time axis by the striking velocity of the pendulum, assuming of course that the striking velocity remains essentially constant throughout the fracture event. The load–deflection traces obtained from the static flexural tests were very similar in shape to the traces obtained from the instrumented Charpy impact tests.

The load–time traces obtained from the instrumented Charpy impact test for the hybrid materials used in the most recent study [3, 4] were also very similar in appearance to the load–time traces previously obtained [1, 2].

The upper photograph of Fig. 1 shows a typical load–time trace for a Modulite 5206 graphite/epoxy control specimen tested in the longitudinal direction. The lower photograph shows a typical load–time trace of a hybrid composite containing discrete plies of S2 glass/epoxy dispersed through-

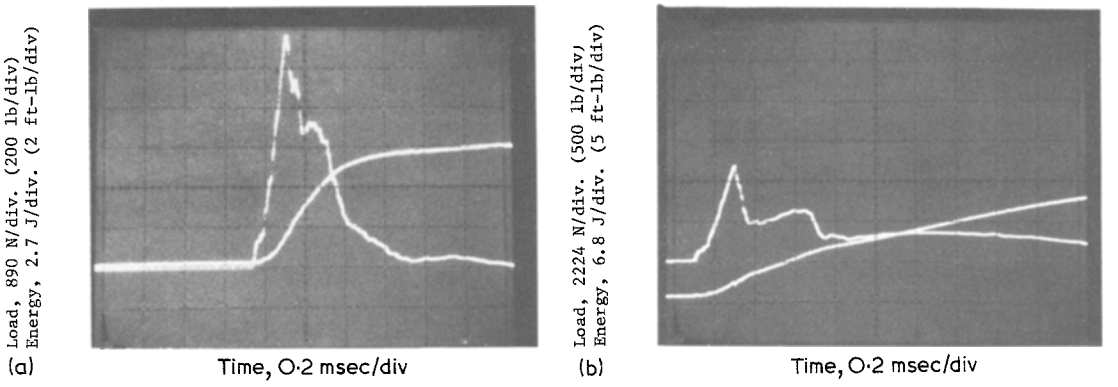

Figure 1 Instrumented impact load and energy wave forms. (a) Modulite 5206 control, longitudinal configuration. (b) Modulite 5206 S2 glass hybrid, longitudinal configuration.

out the thickness of the specimen, also tested in the longitudinal direction. The monotonically increasing trace shown in each of the photographs is the electronic integration of the load–time trace after the load–time curve has been converted to a load–deflection curve, and represents the energy input to the specimen to a given time. Note the difference between the two photographs in terms of the scales of the load and energy values.

It was assumed in the work reported in [5] that no fracture occurred within the test specimen until the point of maximum load had been reached. It was also assumed that the energy represented as the area beneath the load–deflection curve to the point of maximum load equalled the strain energy stored within the specimen. However, depending upon the specific test, the calculations performed in [5] accounted for only approximately 17 to 72% of the total energy represented by the area beneath the load–time trace to the point of maximum load.

All the tests reported in [5] were Charpy impact tests, no static flexure tests being conducted. At that time it was not well-understood whether the additional energy which resulted from integration of the load–deflection curve to the peak load resulted from possible energy dissipation mechanisms unique to impact tests, or if all of the strain energy stored within the specimen had not yet been fully accounted.

A preliminary step toward accounting for all of the energy dissipated by a Charpy impact specimen was taken by calculating the amount of strain energy which is stored within a thick static three-point flexure specimen to the point of initial fracture (i.e. to the point of maximum load). The thick flexure specimens were of the same dimensions as the standard Charpy impact specimens. The same basic procedure as reported in [5] was used to calculate the amount of strain energy stored within a specimen due only to flexure stresses. Some refinements were instituted in the present calculations, however. For example, it was assumed in the previous study that most of the strain energy which was stored by the composite to the point of initial fracture was stored by the fibres, which carry most of the load and thus are at a higher stress than the surrounding epoxy matrix. Therefore, only the longitudinal normal stresses in the direction of the fibres within each lamina of the specimen were considered.

The specimen configuration and co-ordinate

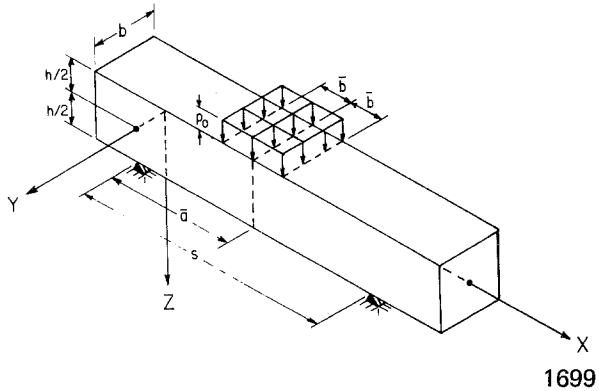

Figure 2 Flexure specimen configuration.

axes arrangement chosen in the current calculations are shown in Fig. 2. The longitudinal normal stress parallel to the fibre direction within each lamina is designated σ_1, while the longitudinal stress parallel to the major axis of the beam is designated σ_x. It was concluded in the present study that the strain energies resulting from the transverse normal stresses σ_2 and the in-plane shear stresses τ_{12} within each ply should also be included. The total strain energy density resulting from the flexure stresses thus becomes

$$\bar{U} = \tfrac{1}{2}\left[\sigma_1^k \epsilon_1^k + \sigma_2^k \epsilon_2^k + \tau_{12}^k \gamma_{12}^k\right] \quad (1)$$

where σ_1^k and ϵ_1^k are the normal stress and strain in the kth ply in the direction parallel to the fibres, and σ_2^k and ϵ_2^k are the normal stress and strain in the kth ply in the direction perpendicular to the fibres. The terms τ_{12}^k and γ_{12}^k are the shear stress and shear strain in the x–y plane of the beam.

Each ply of the laminated composite beam (the test specimen) is considered to be an orthotropic material. Therefore, the strains in the 1- and 2-axis directions are (assuming a plane stress condition) related to the stresses by the generalized Hooke's law as

$$\begin{aligned} \epsilon_1 &= \frac{1}{E_1}\left[\sigma_1 - \nu_{21}\sigma_2\right] \\ \epsilon_2 &= \frac{1}{E_2}\left[\sigma_2 - \nu_{12}\sigma_1\right] \\ \gamma_{12} &= \frac{\tau_{12}}{G_{12}} \end{aligned} \quad (2)$$

where E_1 and E_2 are the elastic moduli in the 1- and 2-axis directions, respectively, G_{12} is the shear modulus in the 1-2 plane, and ν_{12} and ν_{21} are the major and minor Poisson's ratios. Substituting the expressions for the strains of Equation 2 into Equation 1, using the fact that $\nu_{12}/E_2 = \nu_{21}/E_1$, and assuming that the elastic moduli of the plies are the same in tension and compression, one arrives at the following expression for the strain energy resulting from the three flexural stress components, i.e. σ_1, σ_2, and τ_{12}:

$$\bar{U} = \tfrac{1}{2}\left[\frac{(\sigma_1^k)^2}{E_1^k} - \frac{2\nu_{21}^k \sigma_1^k \sigma_2^k}{E_1^k} + \frac{(\sigma_2^k)^2}{E_2^k} + \frac{(\tau_{12}^k)^2}{G_{12}^k}\right]. \quad (3)$$

The strain energy within the beam is then obtained by integrating this expression for strain energy density throughout the total volume of the beam, i.e.

$$\mathbf{U} = \int_0^s \int_A \bar{U}\, dA\, dx \quad (4)$$

where s is the total span length of the beam and A is the cross-sectional area. It is assumed, since the thickness of each individual ply of the laminate is small compared to the total thickness h of the beam, that the stresses are essentially constant throughout the thickness of each ply. The bending moment in the beam is a linear function of the distance x from the end of the beam. Each of the stresses can be expressed as

$$\begin{aligned} \sigma_1^k &= \frac{2\sigma_{1_0}^k x}{s} \\ \sigma_2^k &= \frac{2\sigma_{2_0}^k x}{s} \qquad (0 \leqslant x \leqslant s/2) \\ \tau_{12}^k &= \frac{2\tau_{12_0}^k x}{s} \end{aligned} \quad (5)$$

where $\sigma_{1_0}^k$, $\sigma_{2_0}^k$ and $\tau_{12_0}^k$ are the maximum longitudinal normal, transverse normal and in-plane shear stresses, respectively, developed within the kth ply of the beam, these being located at the midspan cross-section of the beam where the moment for a three-point flexure specimen is maximum. Substituting the expressions for the stresses of Equation 5 into Equation 3, and then using this result in Equation 4, yields the following expression for the strain energy stored within a laminated composite beam due only to the flexure stresses:

$$\mathbf{U} = \frac{s}{6}\sum_{k=1}^{n} A^k \left[\frac{(\sigma_{1_0}^k)^2}{E_1^k} - \frac{2\sigma_{1_0}^k \sigma_{2_0}^k}{E_1^k} + \frac{(\sigma_{2_0}^k)^2}{E_2^k} + \frac{(\tau_{12_0}^k)^2}{G_{12}^k}\right] \quad (6)$$

where A^k is the cross-sectional area of the kth ply of the laminate, s is the total span length of the beam, and n is the total number of plies in the laminate.

The fourth column of Table I lists the values for the strain energy due to flexure stresses for each of the materials and specimen configurations, as calculated using Equation 6 and normalized by dividing the calculated energy values by the cross-

TABLE I Thick flexure specimens: strain energies at failure initiation (normalized)*

Material designation	Specimen configuration	Experimentally determined flexural modulus		Calculated flexural strain energy		Calculated transverse shear strain energy		Total calculated strain energy		Experimental strain energy as integrated beneath the load–deflection curve	
		(GN m^{-2})	(10^6 psi)	(kJ m^{-2})	(ft-lb in.$^{-2}$)	(kJ m^{-2})	(ft-lb in.$^{-2}$)	(kJ m^{-2})	(ft-lb in.$^{-2}$)	(kJ m^{-2})	(ft-lb in.$^{-2}$)
5206 control	longitudinal	40	5.8	7.36	3.5	10.30	4.9	17.66	8.4	17.44	8.3
	transverse	14	2.1	7.78	3.7	8.20	3.9	15.98	7.6	14.92	7.1
5206/120 glass	longitudinal	37	5.3	7.36	3.5	8.41	4.0	15.76	7.5	15.97	7.6
	transverse	17	2.5	7.57	3.6	8.62	4.1	16.18	7.7	15.97	7.6
5206/A1	longitudinal	26	3.8	4.20	2.0	6.94	3.3	11.14	5.3	11.77	5.6
	transverse	13	1.9	6.09	2.9	6.52	3.1	12.61	6.0	11.98	5.7
5206/S2 glass	longitudinal	35	5.1	4.62	2.2	6.31	3.0	10.93	5.2	10.72	5.1
	transverse	15	2.2	6.09	2.9	5.04	2.4	11.13	5.3	10.93	5.2
5206/Ti	longitudinal	6	0.90	0.08	0.04	1.49	0.71	1.57	0.75	1.47	0.70
	transverse	5	0.76	0.11	0.05	0.99	0.47	1.10	0.52	1.05	0.50

* Typically an average of three test specimens.

sectional area of each specimen. Calculations were also performed neglecting the strain energy resulting from the transverse normal stresses and the in-plane shear stresses. It was discovered that the results of including the strain energy developed by the transverse normal stresses and in-plane shear stresses were more pronounced for the transverse specimens than for the longitudinal specimens. For example, the total strain energy calculated for the thick 5206 control specimens in the transverse configurations (normalized by dividing by the cross-sectional area of the specimen) was 7.71 kJ m^{-2} (3.67 ft-lb in.$^{-2}$) when the transverse normal and in-plane shear stresses were included. Only 5.78 kJ m^{-2} (2.75 ft-lb in.$^{-2}$) of normalized strain energy was calculated for this specimen when just the longitudinal normal stresses were considered. However, the calculated strain energy stored within the longitudinal specimens of the 5206 control panel was only increased from 7.12 kJ m^{-2} (3.39 ft-lb in.$^{-2}$) to 7.42 kJ m^{-2} (3.53 ft-lb in.$^{-2}$) when the additional stresses were considered.

The values of the normalized strain energy listed in the fourth column of Table I represent calculations which include the transverse normal stress σ_2 and the in-plane shear stress τ_{12}. The values of the maximum stresses within each ply of the laminate $\sigma^k_{1_0}$, $\sigma^k_{2_0}$ and $\tau^k_{12_0}$, were obtained with the aid of Computer Program AC-3 [6], in the manner described in [1].

The load–deflection curves for the thick static flexure test specimens were all linear to the point of maximum load. (The point of maximum load was assumed to coincide with initial fracture of the specimen.) Therefore, the elastic strain energy (integrated as the area beneath the load–deflection trace) to the point of maximum load can be calculated from the following expression (see any energy methods text):

$$U = \frac{P^2\left(\frac{s}{2}\right)^3}{E_f b h^3} \tag{7}$$

where E_f is the experimentally determined flexural modulus of the beam, P is the maximum load that the specimen can withstand, b is the width of the specimen, and h is the thickness of the specimen, as illustrated in Fig. 2.

The values of the experimentally determined flexural modulus of each material and specimen configuration are listed in the third column of Table I. The values of the energy integrated beneath the load–deflection traces for the thick static flexure specimens are listed in the last column of Table I. It is clear that the calculated values for the strain energy developed from just the flexure stresses within the thick flexure specimens (listed in the fourth column of Table I) are only from 6 to 54% as large as the energy integrated beneath the load–deflection traces. If the results of the Modulite 5206/Ti panels are neglected in the comparison, the values listed in the fourth column are from 40 to 54% as large as the energy values listed in the last column. Neglecting the Modulite 5206/Ti hybrid panel values may be justified since the thick panels of this material

exhibited several anomalous traits associated with excessive delaminations [3, 4].

Ignoring the values of the Modulite 5206/Ti panels, the comparison of the calculated strain energy due only to the flexure stresses to the energy values which represent the energy beneath the load–deflection curve to the point of maximum load is in good agreement with the similar comparison made for the Charpy impact specimens reported in [5]. These calculated strain energies clearly do not account for the total energy obtained by integrating the load–deflection curve to the point of initial fracture. Therefore, it was concluded that either part of the energy beneath the load–deflection curve was dissipated in another manner, or some of the strain energy was as of yet unaccounted.

Data obtained from the "static" flexural test of the thin specimens indicated that transverse shear substantially affected the flexural moduli of the material systems. Although none of the test data for the thin test specimens will be presented here, it was evident, by comparing the flexural moduli values of the thin static flexural specimens to the thick static flexural specimens, that the moduli for the thin specimens were much greater than the moduli for the thick specimens of a corresponding material. As will be seen from the equations derived in the following analysis, the effect of transverse shear strain is to increase the deflection of a specimen tested in flexure, thus reducing the flexural modulus. The transverse shear strain becomes greater as the length-to-depth ratio, s/h, of a specimen decreases, therefore the effective flexural moduli of the thick test specimens were proportionately reduced when compared to the thin specimens.

Also, the thick flexural test specimens failed in a manner which resulted in numerous interlaminar delaminations, indicating the transverse shear stress had exceeded the shear strength of the material. The Charpy impact specimens reported in [1] and [2] also failed in this manner. If the failure had been caused entirely by flexural stresses, then fibre failures would have predominated and a cleavage failure of the specimens would have resulted, with a very small number of delaminations resulting.

Although the thin test specimens which were used in the present study still contained more delaminations than had been expected, the data clearly indicated that the geometry of the test specimens had a definite effect on the test results.

In any case, it seemed logical, since there is no energy dissipating inertia effect associated with the static flexure tests, that the shear strain energy contributed by the transverse shear stresses should be included in the present calculations also.

5. Effects of transverse shear on strain energy

If the assumption is made that only minor amounts of damage occur within the test specimen to the point of initial fracture, then there must exist more stored elastic strain energy within the beam than is accounted for by the flexural stresses alone. One such source of elastically stored energy which hitherto had been ignored is the strain energy associated with the transverse shear strain γ_{xz}.

In order to calculate the strain energy associated with the transverse shear strain, one must be able to evaluate this strain. No means exists, using classical laminated plate theory, to evaluate the shear strain γ_{xz}. Classical laminated plate theory is based on the Kirchoff hypothesis, and the assumption that the plate under analysis is sufficiently thin to be considered in a state of plane stress. Under these conditions the transverse shear strain γ_{xz} is assumed to be negligible. However, Pagano [7] has formulated exact solutions, based on anisotropic elasticity theory, of the behaviour of laminated plates and beams when subjected to cylindrical bending, i.e. when the specimen is assumed to be in a state of plane strain with respect to the x–z plane and the applied transverse traction on the surface of the beam is assumed to be constant in the y-direction (see Fig. 2). Pagano's solutions may be used to arrive at expressions for the displacements associated with a beam, from which the strains may be calculated. If the surface traction is expressed as a Fourier series, Pagano's analysis requires the solution of $4n$ simultaneous algebraic equations. The term n represents the total number of plies in the laminate, and has a value of 60 for the thick hybrid panels considered in the present study. The formulation and subsequent solution of the 240 algebraic equations necessary for each of the materials and specimen configurations used in the present study was considered to be excessive. Therefore, an approximate method, which is based on an extended classical laminated plate theory in which the transverse shear strain may be calculated, was used.

Whitney [8], in formulating this approximate method, has also shown that the solutions representing the behaviour of laminated plate in cylindrical bending are very close to the exact solutions. This approximate method assumes the displacement field in a plate to be

$$\begin{aligned} u &= u^0(x,y) + z\Psi_x(x,y) \\ v &= v^0(x,y) + z\Psi_y(x,y) \\ w &= w(x,y) \end{aligned} \tag{8}$$

where u, v and w are the displacements in the x-, y-, and z-directions, respectively. The quantities Ψ_x and Ψ_y may be viewed as analytic functions from which the plate curvature function Γ may be determined. As will be seen later, these functions must be evaluated such that they are consistent with the boundary conditions of the problem. For cylindrical bending along the x-axis, u^0 and v^0 are the displacements of the midplane of the plate. The strain field is obtained from the classical elasticity definitions relating the displacements and the strains. The strains are:

$$\begin{aligned} \epsilon_x &= \epsilon_x^0 + z\Gamma_x, & \epsilon_y &= \epsilon_y^0 + z\Gamma_y \\ \gamma_{xy} &= \gamma_{xy}^0 + z\Gamma_{xy}, & \gamma_{xz} &= k_1\gamma_{xz}^0, \\ \gamma_{yz} &= k_2\gamma_{yz}^0 \end{aligned} \tag{9}$$

where

$$\begin{aligned} \epsilon_x^0 &= u_{,x}^0 & \epsilon_y^0 &= v_{,y}^0 \\ \gamma_{xy}^0 &= u_{,y}^0 + v_{,x}^0 & \Gamma_x &= \Psi_{x,x} \\ \Gamma_y &= \Psi_{y,y} & \Gamma_{xy} &= \Psi_{x,y} + \Psi_{y,x} \\ \gamma_{xz}^0 &= w_{,x} + \Psi_x & \gamma_{yz}^0 &= w_{,y} + \Psi_y \end{aligned}$$

A subscript comma denotes differentiation with respect to the subscripted variable immediately following it. Whitney calls the terms k_1 and k_2 the shear correction factors; these account for the fact that the transverse shear stress is not uniform throughout each ply of the laminate.

Whitney then substituted the strain and curvature expressions of Equations 9 into the following constitutive relationships derived from classical laminated plate theory:

$$\begin{bmatrix} \bar{\mathbf{N}} \\ \bar{\mathbf{M}} \end{bmatrix} = \left[\begin{array}{c|c} \bar{\mathbf{A}} & \bar{\mathbf{B}} \\ \hline \bar{\mathbf{B}} & \bar{\mathbf{D}} \end{array}\right] \begin{bmatrix} \epsilon^0 \\ \Gamma \end{bmatrix}. \tag{10}$$

The elements of the vector $\bar{\mathbf{N}}$ are the normal forces per unit width applied to the plate, the elements of the vector $\bar{\mathbf{M}}$ are the moments per unit width applied to the plate, ϵ^0 is the midplane strain, and Γ is the curvature function of the plate. The values of the elements of the matrices $\bar{\mathbf{A}}$, $\bar{\mathbf{B}}$, and $\bar{\mathbf{D}}$ are given as

$$[A_{ij}, B_{ij}, D_{ij}] = \int_{-\frac{h}{2}}^{\frac{h}{2}} \bar{Q}_{ij}^k (1, z, z^2)\mathrm{d}z, \quad (i,j = 1,2,6) \tag{11}$$

where $\bar{Q}_{ij}^k$ is an element of the reduced material stiffness matrix of the kth ply. In performing this substitution and expanding the matrix multiplications, Whitney expressed the governing relationships for a plate in cylindrical bending along the x-axis as follows:

$$\begin{aligned} A_{11}u_{,xx}^0 + B_{16}\Psi_{y,xx} &= 0 \\ A_{66}v_{,xx}^0 + B_{16}\Psi_{x,xx} &= 0 \\ k_1^2 A_{55}(\Psi_{x,x} + w_{,xx}) + p &= 0 \\ B_{26}v_{,xx}^0 + D_{11}\Psi_{x,xx} + D_{16}\Psi_{y,xx} & \\ - k_1^2 A_{55}(\Psi_x + w_{,x}) &= 0 \\ B_{16}u_{,xx}^0 + D_{16}\Psi_{x,xx} + D_{66}\Psi_{y,xx} - k_2^2 A_{44}\Psi_y &= 0 \end{aligned} \tag{12}$$

where the coefficients A_{ij}, B_{ij} and D_{ij} are the terms of the $\bar{\mathbf{A}}$, $\bar{\mathbf{B}}$ and $\bar{\mathbf{D}}$ matrices of Equation 10. The term p is the load, i.e. surface traction, distribution along the length of the beam and is a function of x only.

By assuming that the load $p(x)$ is constant in the y-direction, i.e. that the load is symmetrically applied about the x–z plane, then the three-point flexure specimen may be assumed to be in a state of generalized plane strain. The strains in the y-direction, i.e. ϵ_y, γ_{zy} and γ_{xy}, are assumed to be negligible for generalized plane strain conditions. Thus one finds for these conditions, from Equations 9, that $\Psi_y = 0$. The hybrid material systems considered during the present investigation were all symmetric with respect to the midplane of the specimen so that all of the coefficients B_{ij} in Equations 12 are zero.

By definition, the terms D_{16} and D_{26} would be zero if, for every ply above the midplane of a laminate with the fibres oriented at an angle $+\theta$ with respect to the x-direction, there exists a ply below the midplane with the filaments oriented at an opposite angle, $-\theta$, However, symmetrical laminates, such as these used in the present study,

contain plies with the filaments aligned at the same angle at equal distances above and below the midplane. The terms D_{16} and D_{26} will be small, however, if the laminate is constructed such that two adjacent angle plies within the laminate are oriented at opposite angles, and there exists a large number of plies within the laminate. For this type of arrangement, the effects on D_{16} and D_{26} of a ply oriented at an angle $+\theta$ above the midplane will be almost nullified by a ply oriented at an opposite angle $-\theta$ located adjacent to the mirror $+\theta$ ply below the midplane. This was exactly the type of laminate lay-up pattern used in the present study, and the terms D_{16} and D_{26} were relatively small. In fact, for all of the hybrid material systems considered, the terms D_{16} and D_{26} were at least an order of magnitude smaller than the terms D_{11} and D_{66}. Neglecting the terms involving D_{16} and D_{26} in Equations 12, the governing relationships for a beam reduce to

$$A_{11}u^0_{,xx} = 0$$

$$k_1^2 A_{55}(\Psi_{x,x} + w_{,xx}) + p(x) = 0$$

$$D_{11}\Psi_{x,xx} - k_1^2 A_{55}(\Psi_x + w_{,x}) = 0. \quad (13)$$

The boundary conditions for the simply supported flexure specimen shown in Fig. 2 are:

$$w = N_x = N_{xy} = M_x = M_{xy} = 0,$$
$$\text{at} \quad x = 0 \quad \text{and} \quad x = s. \quad (14)$$

A load such as is shown in Fig. 2 may be expanded in a Fourier series as

$$p(x) = \sum_m p_m \sin\frac{m\pi x}{s}, \qquad (m = 1,3,5\ldots). \quad (15)$$

The coefficients of each of the expansion terms are given as

$$p_m = \frac{4p_0}{m\pi}\sin\frac{m\pi\bar{a}}{s}\sin\frac{m\pi\bar{b}}{s}, \qquad (m = 1,3,5\ldots) \quad (16)$$

where p_0 is the load intensity, $\bar{a}$ is the location of the centre of application of the load, and $2\bar{b}$ is the length of the beam over which the load is applied. Pagano and Wang [9] have used the same type of expansion for a similarly loaded beam in applying the exact solutions of [7]. They used a value of $0.02s$ for $\bar{b}$ when approximating a concentrated load at the midspan of the beam and found this value to be quite satisfactory. The value of $\bar{a}$ is $0.5\,s$ for all cases in the present study.

With the load $p(x)$ expanded as shown in Equation 15, solutions to Equations 13 which satisfy the boundary conditions of Equations 14 are:

$$u^0(x) = \sum_m A_m \cos\frac{m\pi x}{s}$$

$$\Psi_x(x) = \sum_m C_m \cos\frac{m\pi x}{s}, \qquad (m = 1,3,5\ldots)$$

$$w(x) = \sum_m E_m \sin\frac{m\pi x}{s} \quad (17)$$

where A_m, C_m and E_m are arbitrary constants which must be determined. The solutions represented by Equations 17 are then substituted into the reduced governing equations of the beam, Equations 13. The first of these equations becomes

$$\sum_m \frac{A_{11}A_m m^2\pi^2}{s}\cos\frac{m\pi x}{s} = 0,$$
$$(m = 1,3,5\ldots). \quad (18)$$

Since each term $\cos(m\pi x/s)$ is not, in general, zero for all values of x along the length of the beam, the only way Equation 18 can be true for all values of x is if each of the coefficient terms is zero, i.e. if

$$\frac{A_{11}A_m m^2\pi^2}{s} = 0, \qquad (m = 1,3,5\ldots). \quad (19)$$

However, A_{11} and m are never zero, so it follows that $A_m = 0$ for all m, and therefore $u^0(x) = 0$. The last two of Equations 13 have the form

$$\sum_m \left[p_m - \frac{k_1^2 A_{55}m\pi}{s}\left(C_m - \frac{E_m m\pi}{s}\right)\right]\sin\frac{m\pi x}{s} = 0$$

and

$$\sum_m \left[\left(\frac{D_{11}m^2\pi^2}{s^2} + k_1^2 A_{55}\right)C_m + \frac{m\pi k_1^2 A_{55}E_m}{s}\right]$$
$$\cos\frac{m\pi x}{s} = 0. \quad (20)$$

Again, each of the coefficients of the terms $\sin(m\pi x/s)$ and $\cos(m\pi x/s)$ must vanish for each value of m. Therefore, each of the coefficients C_m and E_m can be expressed in terms of the load coefficients p_m as follows:

$$C_m = -\frac{p_m s^3}{m^3\pi^3 D_{11}} \quad (21)$$

and

$$E_m = \frac{p_m s^2}{m^2\pi^2}\left(\frac{1}{k_1^2 A_{55}} + \frac{s^2}{m^2\pi^2 D_{11}}\right).$$

Thus, the solutions to the governing equations of the beam, Equation 13 become

$$u^0 = 0$$

$$\Psi_x = -\sum_m \frac{p_m s^3}{m^3\pi^3 D_{11}} \cos\frac{m\pi x}{s},$$

$$(m = 1, 3, 5\ldots)$$

$$w = \sum_m \frac{p_m s^2}{m^2\pi^2}\left(\frac{1}{k_1^2 A_{55}} + \frac{s^2}{m^2\pi^2 D_{11}}\right)\sin\frac{m\pi x}{s} \quad (22)$$

where the values of p_m are given by Equation 16.

The strain energy density of the kth ply resulting from the transverse shear strains developed in a flexure specimen assumed to be in cylindrical bending is

$$\bar{U}^k = \tfrac{1}{2}k_1^2 \bar{Q}_{55}^k (\gamma_{xz}^0)^2 = \tfrac{1}{2} G_{xz}^k (\gamma_{xz}^k)^2. \quad (23)$$

The transverse shear strain energy in the kth ply is thus

$$U^k = \int_{z_{k-1}}^{z_k}\int_0^b\int_0^s \tfrac{1}{2}k_1^2 \bar{Q}_{55}^k (\gamma_{xz}^0)^2 \, dx\, dy\, dz. \quad (24)$$

Since the shear correction factor k_1 is a constant and the function γ_{xz}^0 is a function of x only, for a beam in cylindrical bending, integration of Equation 24 in the z- and y-directions may be readily carried out to yield the following expression:

$$U^k = \tfrac{1}{2}(z_k - z_{k-1})\bar{Q}_{55}^k k_1^2 b \int^s (\gamma_{xz}^0)^2 \, dx \quad (25)$$

where $(z_k - z_{k-1})$ is the thickness of the kth ply, the plies being numbered starting from the $z = -(h/2)$ surface of the beam. The terms given in Equations 22 may now be used to expand the definition of γ_{xz}^0 given in Equations 9 to yield the following expression:

$$\gamma_{xz}^0 = \sum_m \left[\left(\frac{m\pi E_m}{s} + C_m\right)\cos\frac{m\pi x}{s}\right],$$

$$(m = 1, 3, 5\ldots) \quad (26)$$

where E_m and C_m are evaluated using Equation 21. By substituting Equation 26 into Equation 25, the expression for the transverse strain energy within the kth ply becomes

$$U^k = \tfrac{1}{2}(z_k - z_{k-1})\bar{Q}_{55}^k k_1^2 b \int_0^s \sum_m \left[\left(\frac{m\pi E_m}{s} + C_m\right)\cos\frac{m\pi x}{s}\right]^2 dx,$$

$$(m = 1, 3, 5\ldots). \quad (27)$$

It follows that the strain energy due to the transverse shear stress in a laminated beam is the sum of the energies within each ply. The expression for the transverse shear strain energy is

$$U = \sum_{k=1}^n U^k = \sum_{k=1}^n \tfrac{1}{2}(z_k - z_{k-1})\bar{Q}_{55}^k k_1^2 b \int_0^s \sum_m \left[\left(\frac{m\pi E_m}{s} + C_m\right)\cos\frac{m\pi x}{s}\right]^2 dx,$$

$$(m = 1, 3, 5\ldots). \quad (28)$$

An expansion of Equation 11 shows that the definition of the material parameter A_{55} is as follows:

$$A_{55} = \sum_{k=1}^n (z_k - z_{k-1})\bar{Q}_{55}^k. \quad (29)$$

The total transverse shear strain energy expression for a three-point flexure specimen thus becomes

$$U = \tfrac{1}{2}A_{55}k_1^2 b \int_0^s \sum_m \left[\left(\frac{m\pi E_m}{s} + C_m\right)\cos\frac{m\pi x}{s}\right]^2 dx,$$

$$(m = 1, 3, 5\ldots). \quad (30)$$

The terms of the summation within the brackets of the integral are orthogonal over the interval $0 \leqslant x \leqslant s$. Therefore, all cross-product terms such as $\cos(m\pi x/s)\cos[m+1)\pi x/s]$ integrate to zero over the interval $0 \leqslant x \leqslant s$. The integration of Equation 30 may thus be readily performed, resulting in the following final form for the expression of the transverse shear strain energy:

$$U = \frac{A_{55}k_1^2 bs}{4}\sum_m \left(\frac{m\pi E_m}{s} + C_m\right)^2,$$

$$(m = 1, 3, 5\ldots) \quad (31)$$

where s is the length of the beam, b is the width, and A_{55} is a material parameter of the beam defined in Equation 29, and readily available from calculations performed in Computer Program AC-3.

At this point, all of the variables and material parameters are available except a value for the shear correction factor k_1. Whitney has shown that the value of the shear correction factor k_1 is a function of the orientation of the plies within the beam and the material properties of each ply [8]. Therefore, a value of k_1 for each material system and specimen configuration must be calculated in order to determine the contribution of the transverse shear strain energy to the strain energy stored within the given beam.

The value of the shear correction factor k_1 can be determined either analytically or by experimental means. Whitney [8] has described a method of calculating the value of k_1 which requires the solution of $n + 1$ simultaneous algebraic equations. Bert [10] has derived a method different than Whitney's for analytically calculating the values of k_1 for beams subjected to cylindrical bending. Bert's method reduces to one single expression for determining k_1. However, the expression contains functions which he has defined as the partial stiffness of the beam, and must be generated in the present investigation, the analytical methods of determining k_1 were forgone in wise continuous for laminated beams in which the individual plies have different physical properties.

The experimental method of calculating the shear correction factor k_1 is much more straightforward, and requires far less complex calculations. Since the experimental data which are needed to calculate the shear correction factors were already generated in the present investigation, the analytical methods of determining k_1 were forgone in favour of the experimental technique.

The experimental technique of determining the shear correction factor k_1 consisted of accounting for the transverse shear effects on the value of the flexural moduli of the specimens when subjected to three-point flexure loadings. First, the flexural modulus for each material and specimen configuration was calculated using the experimentally determined deflection and load in the following equation:

$$E_f = \frac{s^3\left(\frac{P}{\delta}\right)}{4bh^3} \tag{32}$$

where P is the applied load and δ is the midspan deflection. The load–displacement curves of the flexure test supplied the data necessary for these calculations. The last column of Table II lists the values of the flexural moduli of the thick test specimens, as calculated using the experimental values from the load–deflection curves. The deflection δ of the flexure specimen at the midspan is equal to w, as defined in the third of Equations 22, evaluated at the midspan, i.e. at $x = s/2$. The flexural modulus of the beam may thus be analytically determined by calculating δ for an arbitrary load p_0, then using these values in Equation 32.

The value of the shear correction factor k_1 was determined for each material system and specimen configuration by iterating through a range of values of k_1 until the calculated flexural modulus, obtained from the analytically determined midspan deflection, matched the experimentally determined value.

The value of the shear correction factor for each of the thick specimens is listed in the sixth column of Table II. The values of the material parameters A_{55} and D_{11}, required in the calculations of Equations 22, are listed respectively

TABLE II Analytically determined flexural moduli of thick static flexure specimens

Material designation	Specimen configuration	Flexural modulus calculated using Equation 33		A_{55}		D_{11}		k_1	Flexural modulus calculated using Equation 32	
				(MN m^{-1})	(10^5 lb in.$^{-1}$)	(kN-m)	(10^4 in.-lb)			
		(GN m^{-2})	(10^6 psi)						GN m^{-2})	(10^6 psi)
5206	longitudinal	88	12.8	36.8	2.1	3.2	2.8	0.66	40	5.8
control	transverse	19	2.7	28.0	1.6	0.9	0.8	0.48	14	2.1
5206/120	longitudinal	71	10.3	38.5	2.2	2.6	2.3	0.64	37	5.3
glass	transverse	23	3.3	33.3	1.9	1.0	0.9	0.51	17	2.5
5206/A1	longitudinal	62	9.0	50.8	2.9	2.9	2.6	0.51	26	3.8
	transverse	19	2.7	43.8	2.5	1.1	1.0	0.42	13	1.9
5206/S2	longitudinal	77	11.1	36.8	2.1	2.7	2.4	0.62	35	5.1
glass	transverse	19	2.7	28.0	1.6	0.9	0.8	0.53	15	2.2
5206/Ti	longitudinal	85	12.4	68.3	3.9	5.9	5.2	0.21	6.2	0.9
	transverse	39	5.7	61.3	3.5	3.1	2.7	0.21	5.5	0.8

in the fourth and fifth columns of Table II.

An additional point of interest is the actual amount by which the transverse shear strain affects the calculations of the flexural modulus for composite beams. Using classical laminated plate theory, which neglects transverse shear strain effects, and neglecting Poisson effects, an expression for the flexural modulus can be shown to be [3]

$$E_f = \frac{\sum_{k=1}^{n} E_1^k (z^k)^2 A^k}{I} \quad (33)$$

where E_k is the tensile modulus of the kth ply, z_k is the distance from the midplane of the beam to the kth ply, and A_k is the cross-sectional area of the kth ply. The term I is the moment of inertia of the entire cross-section of the beam.

The values of the flexural modulus of the various thick flexure specimens as calculated using Equation 33 are listed in the third column of Table II. It is evident by comparing the values of the third column to the values of the last column of Table II that the transverse shear strains reduce the flexural modulus of a beam. The difference is most evident for the longitudinal specimen configurations. The deformations due to the transverse shear stress are usually more pronounced for highly anisotropic beams. One measure of the degree of anisotropy of the material, which is important in characterizing the amount of deformation of the material, is the ratio of the longitudinal tensile modulus E_x to the longitudinal-transverse shear modulus G_{xz}. This ratio, E_x/G_{xz}, was much larger for the longitudinal specimens of the present study than for the transverse specimens, thus the transverse shear effects were much more pronounced for the longitudinal specimens.

The values of the shear correction factor k_1 for each of the material systems, for the thick static flexure specimens as listed in the sixth column of Table II, were used in the calculation of the strain energy due to transverse shear strains (Equation 31). The calculated values of the strain energy due to transverse shear strain effects are listed in the fifth column of Table I.

The sums of the flexural strain energy (listed in the fourth column of Table I) and the transverse shear strain energy (listed in the fifth column) are tabulated in the sixth column. The comparison of the calculated values of the strain energy to the energy represented by the area beneath the load–deflection curve to the point of maximum load is quite good. This indicates that, for the thick static flexure specimens used in this study, which have an s/h ratio of approximately four, at least half of the strain energy stored within the specimens was transverse shear strain energy. The good comparison between the values in the sixth and seventh columns of Table I indicates that all of the energy represented beneath the load–deflection curve for the static flexure specimens is stored as strain energy within the beam. With this fact in hand, a better evaluation of the Charpy impact tests can be made.

6. Energy associated with the Charpy impact test

The behaviour of the hybrid material systems subjected to impact, as studied during the present investigation, was more amenable to analysis than in previous investigations because direct correlations could be made with the behaviour of identical specimens subjected to three-point static flexural loadings. A few of these comparable quantities are the flexural modulus, the initial fracture energy (obtained by integrating the area under the load–deflection trace to the point of maximum load, i.e. to the point of assumed initial fracture), the maximum load, and the energy dissipated in the total failure of the specimen.

A substantial difference in behaviour occurred between the Charpy impact specimens and the static flexure specimens, for all of the material systems considered in this investigation. The distinction was present in both the thick and thin test specimens. One of the most obvious manifestations of the difference in behaviour was the difference in the amount of energy which was obtained by integrating the load–deflection trace to the point of maximum load. These energy values, normalized by dividing by the specimen cross-sectional area, for the thick Charpy impact specimens, are listed in the fourth column of Table III. The energy values obtained by integrating the load–deflection curve to the point of maximum load, then normalizing by dividing by the cross-sectional area of the specimen, for the "static" flexure tests of the thick specimens, are repeated from Table I in the third column of Table III.

It is clear that the amount of initial fracture energy associated with the Charpy impact specimens of each material system was always greater than the similar energy associated with the

TABLE III Initial fracture energies (normalized) and peak loads of the thick Charpy impact and static flexure specimens*

Material designation	Specimen configuration	Static flexure initial fracture energy		Charpy impact initial fracture energy		Static flexure peak load		Charpy impact peak load	
		(kJ m^{-2})	(ft-lb in.$^{-2}$)	(kJ m^{-2})	(ft-lb in.$^{-2}$)	(kN)	(lb)	(kN)	(lb)
5206 control	longitudinal	17.44	8.3	29.00	13.8	4.96	1114	5.13	1153
	transverse	14.92	7.1	14.29	6.8	2.84	638	2.18	491
5206/120	longitudinal	15.97	7.6	29.84	14.2	4.43	996	4.27	960
glass	transverse	15.97	7.6	22.07	10.5	3.09	694	2.74	615
5206/Al	longitudinal	11.77	5.6	20.17	9.6	3.83	861	4.14	930
	transverse	11.98	5.7	15.97	7.6	2.90	651	2.86	643
5206/S2	longitudinal	10.72	5.1	21.02	10.0	3.67	824	4.43	997
glass	transverse	10.93	5.2	10.30	4.9	2.43	546	2.06	464
5206/Ti	longitudinal	1.47	0.7	13.66	6.5	0.92	207	1.31	295
	transverse	1.05	0.5	2.52	1.2	0.70	158	0.79	178

* Typically an average of three test specimens.

corresponding static flexure specimens. Also, the difference between the initial fracture energy of the Charpy impact specimens and the static flexure specimens was greater for the longitudinal configuration than it was for the transverse beams. The initial fracture energy values associated with the longitudinal static flexure specimens were typically only 53 to 60% as large as the corresponding values for the Charpy impact specimens. One exception was the ratio of these corresponding energies for the Modulite 5206/Ti hybrid material system, which was exceptionally low at only 11%. The initial fracture energy values for the transverse static flexure specimens were, in general, from 72 to 106% as large as the corresponding values for the Charpy specimens of the same configuration, with the Modulite 5206/Ti hybrid system again yielding an abnormally low value.

The increased amount of energy which can be input to a Charpy impact specimen relative to a static flexure specimen is apparently not a function of the thickness of the specimen. The specimens which were cut from the thin panels were all of the longitudinal configuration. Although not listed here, the ratio of the initial fracture energy values for the Charpy impact tests were, for most of the thin panels, within the same range as the ratios for the longitudinal thick specimens [3].

The load–deflection traces were linear to the point of maximum load for both tests. Therefore, in order to account for the greater amount of energy absorbed by the Charpy specimens, a study of the peak loads sustained by each specimen in both types of tests was made. The average values of the peak loads for the static three-point flexure specimens are listed in the fifth column of Table III, and the corresponding values for the Charpy impact specimens are listed in the sixth column of the same table. The average peak loads for the Charpy impact specimens were not substantially greater than the corresponding loads for the static flexure specimens. In fact, as can be seen from Table III, some of the average peak loads for the static flexure specimens were actually even greater than the values for the Charpy impact specimens. A comparison of the average of all of the peak loads for the Charpy impact specimens with the average of all of the peak loads for the static flexure specimens shows that the value of the latter is only about three percent less than the average value of all of the peak impact loads.

The difference in the initial fracture energies of the Charpy impact specimens and the static flexure specimens is evidently attributable to a difference between the flexure modulus of the two types of test specimens. Fig. 3 is an illustration

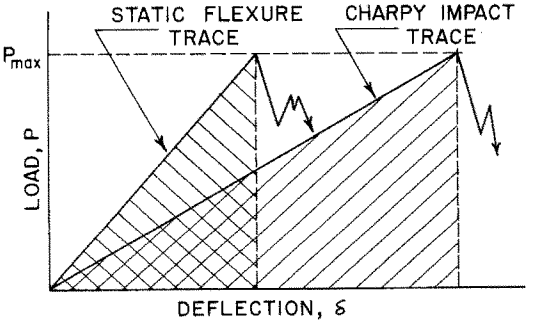

Figure 3 Comparison of the initial portion of a typical static flexure trace and a corresponding Charpy impact trace.

of typical load–deflection traces (reduced to the same scale) for a Charpy impact test and a static flexure test of identical specimens. The traces are both linear to the point of maximum load, and the peak loads are typically approximately equal; but the energy of the Charpy impact specimen, which is represented as the area under the trace, is greater than the energy associated with the flexure specimen. The energy associated with the impact test is greater because the flexural modulus of the impact specimen is less than the modulus of the static flexure specimen. It is believed that this observation may be significant to the eventual explanation of the mechanisms controlling the impact event. Although the present conclusions are felt to be somewhat premature, further investigation is expected to disclose the full nature of the parameters involved.

7. Discussion

It is clear, from the analysis shown here, that the transverse shear stresses occupy a major role in the behaviour of both the dynamic and static flexure tests for specimens of the standard Charpy impact specimen geometry. These effects increase the amount of midspan deflection in both the static and impact three-point flexure tests. The analysis has shown that at least half of the total strain energy which is stored within a flexure specimen of the geometry of a standard Charpy impact specimen, when subjected to a "static" flexural loading, is due to the transverse shear strain.

The calculations performed here also strengthen the supposition that, for static three-point flexure tests, the energy integrated beneath the load–deflection trace to the point of maximum load is stored strain energy within the specimen, and only a minimal amount of energy is dissipated in damage before the peak load is attained. From these results it may be concluded that the most significant material characteristics of hybrid composites may not be adequately emphasized by using a beam specimen of the dimensions of the standard Charpy specimen. That is, the important material characteristics which are needed for impact design purposes may be masked by the transverse shear effects introduced by the small s/h ratios of the Charpy specimens.

The limitations of the Charpy-type impact test discussed here are consistent with those which have long made the use of the flexure test for measuring the static properties of composite materials questionable. That is, the highly anisotropic nature of the composite, combined with the often grossly different mechanisms of failure in tension (cleavage, fibre debonding, fibre pull-out) and compression (ply buckling, fibre micro-buckling, shear crushing), typically lead to a very unpredictable failure mode. This is further complicated in a very small s/h ratio specimen by the complex local stress states induced at the points of load application and specimen support. The short thick specimen requires a relatively high applied force to cause failure, but allows little length over which to uniformly redistribute this concentrated force.

The use of a thinner specimen in the present study does not appear to be the proper solution. Although some of the above disadvantages were reduced, the general limitations remained. The authors and their colleagues have experimented with the use of a tensile impact test as a means of obtaining a simple stress state. This, of course, can be augmented by compressive impact and pure shear impact tests, in order to fully characterize a composite material. While results to date [11] have not been satisfactory because of specimen gripping problems, the concept appears to be sound. The further work being planned should resolve these problems. The use of a tensile impact test would eliminate many of the problems discussed above, and make the use of a relatively complex analysis such as presented here unnecessary. However, until the Chapry impact test, and the somewhat similar Izod impact test, both long time industry standards, are displaced, the problem of attempting to interpret the results obtained will remain.

It was particularly interesting that the hybrid composite materials evaluated in the present study were able to sustain approximately the same amount of load when impacted as when loaded quasi-statistically. However, these materials deflected much more before fracture occurred when subjected to impact loadings, thus the integration of the impact load–deflection trace to the point of maximum load resulted in much more energy than the corresponding energy of a static flexure test. This was not an isolated observation, however. The same trend has been noted in our prior investigation [1, 5], and confirmed by the published results of others [12]. Thus, there appears to be little question as to the reliability of the data. Among these various studies, a wide range

of material configurations have been tested.

The reason for the greater amounts of energy beneath the load–deflection trace for the impact tests as compared to the static tests is as yet indefinite. However, strong indications place the cause of this type of observed behaviour on some rate dependent behaviour of the constitutive materials of the composite. It has been proposed by Harris [13] that the non-uniform interlaminar shear stresses induced in composite plates (or beams) of finite width may be a contributing factor. He suggests that the large shear stresses which are developed at the free edges can be dissipated somewhat by creep in the polymer matrix in a "static" flexure test, while at high loading rates there will be no time for this to occur. Harris supports this possibility with his observation that the interlaminar shear strength of a composite decreased with increased rate of loading. Obviously, this entire rate dependency aspect will require considerably more study. It is interesting, however, that Plenger [11] also noted a rate dependence in his axial tensile static and impact tests of unidirectionally-reinforced graphite/epoxy and glass/epoxy composites. In these tests the effects of shear stresses would presumably be small.

Inertia effects as a possible cause of the observed behaviour are highly unlikely since these types of effects should appear as sharp spikes in the initial portion of the load–time traces, which although they would add to the energy to the point of maximum load, could still be detected. No such sharp spikes were observed in the initial portions of the present load–time traces.

In order to actually account for the additional energy involved in the impact event as compared to the static flexure test, it may be necessary to first evaluate the rate dependence of the constituent materials of the hybrid composite.

Acknowledgements

The investigation upon which this paper is based was sponsored by the Naval Air Systems Command, Washington, D.C., under the direction of Mr Maxwell Stander. The authors wish to thank Mr J. L. Perry of the Aeronutronic Division of Aeronutronic Ford Corporation, who generated all of the experimental data used here.

References

1. J. L. PERRY, J. L. KIRKHART and D. F. ADAMS, Final Report, Naval Air Systems Command, Contract N00019-73-C-0389, Aeronutronic Division, Philco-Ford Corporation, March 1974.
2. J. L. PERRY and D. F. ADAMS, *Composites* **6** (1975) 166.
3. J. L. PERRY, D. F. ADAMS and A. K. MILLER, Final Report, Naval Air Systems Command, Contract N00019-74-C-0229, Aeronutronic Division, Philco-Ford Corporation, January 1975.
4. D. F. ADAMS and J. L. PERRY, *J. Testing and Evaluation*, **5** (2) (1977).
5. D. F. ADAMS and A. K. MILLER, *Mat. Sci. Eng.* **19** (1975) 245.
6. "Advanced Composites Design Guide, Volume II – Analysis," 3rd Edn., (Air Force Materials Laboratory, Dayton, Ohio, January 1973).
7. N. J. PAGANO, *J. Comp. Mater.* **3** (1969) 398.
8. J. M. WHITNEY, *ibid* **6** (1972) 426.
9. N. J. PAGANO and A. S. D. WANG, Report No. AFML-TR-71-143, Air Force Materials Laboratory, October 1971.
10. C. W. BERT, *J. Comp. Mater.* **7** (1973) 525.
11. J. H. PLENGER, M. S. Thesis, University of Wyoming, December 1975.
12. L. J. BROUTMAN and P. K. MALLICK, Air Force Office of Scientific Research Report AFOSR-TR-75-0472, Illinois Institute of Technology, November 1974.
13. B. HARRIS, "Carbon Fibres in Engineering", edited by M. Langley, (McGraw-Hill, London, 1973) pp. 27–28.

Received 28 October 1975 and accepted 16 February 1976.